

# **ARTICLE TYPE**

Cite this: DOI: 00.0000/xxxxxxxxxx

# Time-resolved momentum imaging of UV photodynamics in structural isomers of iodopropane probed by site-selective XUV ionization<sup>†</sup>

Felix Allum,  ${}^*a,b,c$  Yoshiaki Kumagai,  ${}^d,e$  Kiyonobu Nagaya,  ${}^f$  James R. Harries,  ${}^g$  Hiroshi Iwayama,  ${}^{h,i}$  Mathew Britton,  ${}^c$  Philip H. Bucksbaum,  ${}^b$  Michael Burt,  ${}^{j,k}$  Mark Brouard,  ${}^j$  Briony Downes-Ward,  ${}^l$  Taran Driver,  ${}^c$  David Heathcote,  ${}^j$  Paul Hockett,  ${}^m$  Andrew J. Howard,  ${}^b$  Jason W. L. Lee,  ${}^a$  Yusong Liu,  ${}^b$  Edwin Kukk,  ${}^n$  Joseph W. McManus,  ${}^j$  Dennis Milešević,  ${}^j$  Russell S. Minns,  ${}^l$  Akinobu Niozu,  ${}^o$  Johannes Niskanen,  ${}^n$  Andrew J. Orr-Ewing,  ${}^p$  Shigeki Owada,  ${}^q,{}^r$  Patrick Robertson,  ${}^j,{}^s$  Daniel Rolles,  ${}^t$  Artem Rudenko,  ${}^t$  Kiyoshi Ueda,  ${}^u$  James Unwin,  ${}^j$  Claire Vallance,  ${}^j$  Tiffany Walmsley,  ${}^j$  Michael N. R. Ashfold  ${}^p$  and Ruaridh Forbes\*  ${}^c,{}^v$ 

Received Date Accepted Date

DOI: 00.0000/xxxxxxxxxx

The photodynamics of 1- and 2-iodopropane (1 and 2-IP) were studied in a time-resolved scheme incorporating ultraviolet (UV) excitation and extreme ultraviolet (XUV) probing, which initiates photoionization selectively from the I 4d core orbital. UV absorption in the A band of both isomers leads to prompt C-I bond fission, with significant disposal of internal energy into the propyl radical product. Site-selective ionization enables a range of charge transfer (CT) processes between the nascent highly charged iodine ions and neutral propyl radicals, dependent on the interfragment distance at the instant of ionization. Subtle differences in the dynamics of these CT processes between the two isomers are observed. In 1-IP, the kinetic energies of iodine ions produced by UV photodissociation and subsequent XUV multiple ionization increased over the first few hundred femtoseconds, which could be understood in terms of differing gradients along the photodissociation coordinates of the neutral and polycationic states involved in the pump and probe steps, respectively. Led by a recent report of HI elimination in UV photoexcited 2-IP [Todt et al., Phys. Chem. Chem. Phys., 22(46), 27338 (2020)], we also model the most likely signatures of this process in the present experiment, and can identify signal (which is absent or significantly weaker in the data from the unbranched 1-IP isomer) that is consistent with such a process occurring on ultrafast timescales.

 $<sup>^</sup>a$  Deutsches Elektronen-Synchrotron DESY, Notkestraße<br/>85, 22607 Hamburg, Germany. E-mail: felix.allum@desy.de

<sup>&</sup>lt;sup>b</sup> PULSE Institute, SLAC National Accelerator Laboratory, 2575 Sand Hill Road, Menlo Park, CA 94025, USA.

<sup>&</sup>lt;sup>c</sup> Linac Coherent Light Source, SLAC National Accelerator Laboratory, 2575 Sand Hill Road, Menlo Park, CA 94025, USA.

<sup>&</sup>lt;sup>d</sup> Department of Applied Physics, Tokyo University of Agriculture and Technology, Tokyo, Japan.

<sup>&</sup>lt;sup>e</sup> Department of Physics, Nara Women's University, Nara 630-8506, Japan.

<sup>&</sup>lt;sup>f</sup> Department of Physics, Kyoto University, Kyoto 606-8502, Japan.

g QST, SPring-8, Kouto 1-1-1, Sayo, Hyogo, Japan.

<sup>&</sup>lt;sup>h</sup> Institute for Molecular Science, Okazaki 444-8585, Japan.

i Sokendai (The Graduate University for Advanced Studies), Okazaki 444-8585, Japan.

 $<sup>^{\</sup>it j}$  Chemistry Research Laboratory, Department of Chemistry, University of Oxford, Oxford OX1 3TA, United Kingdom.

<sup>&</sup>lt;sup>k</sup> Department of Chemistry, Trent University, Peterborough, ON K9L 0G2, Canada.

<sup>&</sup>lt;sup>1</sup> School of Chemistry and Chemical Engineering, University of Southampton, Southampton, SO17 1BJ, United Kingdom.

 $<sup>^{\</sup>it m}$  National Research Council of Canada, 100 Sussex Dr. Ottawa, ON K1A 0R6, Canada.

 $<sup>^{\</sup>it n}$  Department of Physics and Astronomy, University of Turku, FI-20014 Turku, Finland.

 $<sup>^{</sup>o}$  Graduate School of Humanities and Social Sciences, Hiroshima University, Higashi-

## 1 Introduction

Methyl iodide, the simplest alkyl iodide, has been studied extensively in the field of gas-phase chemical physics. It serves as a prototypical molecule for the study of photodissociation in polyatomic molecules and a benchmark for new experimental probes of photodissociation dynamics 1-13. Excitation in the broad and structureless A-band (centred at ~260 nm) primarily populates the dissociative 3Q0 state, ultimately leading to formation of spin-orbited excited (I\*) and ground state (I) atomic iodine products, along with their CH3 partners, on an ultrafast ( $\sim$ 100 fs <sup>14</sup>) timescale. The latter products (I+CH<sub>3</sub>) are formed following non-adiabatic coupling via a conical intersection to the <sup>1</sup>Q<sub>1</sub> state. More complex alkyl iodides exhibit similar A-band absorption spectra 15 but have garnered less attention. However, a number of studies have highlighted how the increased structural complexity, and consequent increase in the number of nuclear degrees of freedom lead to rich photodissociation dynamics 16-18. These dynamics have been recently interrogated on ultrafast timescales by Bañares and coworkers with femtosecond time-resolved velocity-map imaging (VMI) following excitation at 268 nm<sup>19</sup> and by Leone and coworkers using transient XUV transient absorption spectroscopy following excitation in the range 277-280 nm <sup>13,20,21</sup>. Notably, the I:I\* photoproduct branching ratio varies significantly across the alkyl iodide family, with larger and more branched molecules favouring I product formation through the non-adiabatic pathway <sup>18,19,22–25</sup>. Motions along coordinates other than the C-I stretch also become of greater importance, as indicated by the greater funneling of energy into internal modes of the alkyl radical products, leading to broader product kinetic energy (KE) distributions that peak at lower values <sup>19</sup>. This truly multidimensional nature of the photodynamics is in stark contrast to methyl iodide, which, from a fragmentation perspective, is often viewed as a 'pseudo diatomic' system.

A recent study by Davis and coworkers using photofragment translational energy spectroscopy explored the role of HI elimination following UV excitation of 1-IP and 2-IP (structures shown in Fig. 1)<sup>22</sup>. Here, possible photoproducts were mass-spectrometrically detected following ionization either by electron impact or using nanosecond vacuum ultraviolet (VUV) laser pulses. In the case of 2-IP, significant UV-induced HI signal was observed (via the HI<sup>+</sup> ion), as had been reported by a previous mass spectrometry study into the photochemistry of several iodoalkanes<sup>26</sup>. The detected HI<sup>+</sup> ions had a very similar kinetic

Hiroshima, 739-8524, Japan.

energy and angular distribution to that of the ground state I atom photoproducts. From the observed anisotropic HI<sup>+</sup> angular distribution (anisotropy parameter,  $\beta = 1.92$ ), it was inferred that HI elimination occurred on ultrafast (sub-picosecond) timescales, prior to significant rotation of the parent. The branching ratio for HI elimination from 2-IP was estimated at 10.5%. In comparison, 1-IP showed no such signatures, and an upper-limit branching ratio of 0.21% was estimated for HI elimination from 1-IP. It was speculated that this clear preference for HI elimination from the branched species reflected differences in the internal motion of the recoiling C<sub>3</sub>H<sub>7</sub> radical following C-I bond cleavage. In the case of 2-IP, 'umbrella-like' out-of-plane bending motion of the C<sub>3</sub>H<sub>7</sub> radical bring the secondary hydrogens towards the recoiling iodine atom, resembling motion along the reaction coordinate for HI formation. In contrast, the arcing motion of the secondary hydrogen atoms in the rotating C<sub>3</sub>H<sub>7</sub> photofragment produced from 1-IP was proposed to be nearly orthogonal to the reaction coordinate for HI formation <sup>22</sup>.

Small iodine-containing organic molecules have also recently been popular targets in emerging studies of ultrafast charge transfer (CT) in ionized dissociating molecules 27. In these experiments, ultrafast C-I bond cleavage is induced, either by singlephoton UV or multiphoton near-infrared (NIR) excitation, prior to ionization with a short-wavelength pulse in the extreme ultraviolet (XUV) or X-ray region produced by a free-electron laser (FEL). By choosing a suitable photon energy, ionization can be induced selectively at a specific atomic orbital within the dissociating system, typically those belonging to the I atom. At long pumpprobe time delays (and consequently, large distances between the recoiling photoproducts), low KE  $I^{n+}$  ions are observed. Such signal is absent at short pump-probe delays, however, as a result of CT from the  $I^{n+}$  to the recoiling co-fragment  $^{27}$ . Following CT, mutual Coulomb repulsion between the two ions significantly raises their KEs. For higher charge iodine ions, CT is possible over greater internuclear separations, and so the rise in intensity of the lower KE  $I^{n+}$  ions typically occurs at longer pump-probe delays. This charge state dependence is often rationalized more quantitatively in terms of the classical over-the-barrier (OTB) model <sup>27–29</sup>, wherein CT is assumed to occur up to a certain 'critical distance' between the separating partners, determined by the ionization potential of the site donating the electron and the charge state of the electron-accepting species. After the initial demonstration of this pump-probe approach to studying ultrafast CT dynamics <sup>27</sup>, the concept has been extended to study several different alkyl and aryl iodides pumped in various schemes 12,30-36. Our collaboration recently observed high KE ions produced through CT in UVexcited 2-IP, and demonstrated that detailed analysis of this signal as a function of pump-probe delay and of KE can yield significant insights into how CT probabilities depended on the interfragment separation and  $I^{n+}$  charge state  $^{37}$ .

Here, we present a comparative UV pump - XUV probe study of the photochemistry and CT dynamics of the structural isomers 1- and 2-IP. By measuring three-dimensional ion momenta as a function of the time-delay between the two pulses, the experiment probes both UV-induced photochemistry and XUV-induced CT processes. We observe ultrafast photodissociation dynamics

 $<sup>^{</sup>p}$  School of Chemistry, University of Bristol, Cantock's Close, Bristol BS8 1TS, United Kingdom.

<sup>&</sup>lt;sup>q</sup> RIKEN SPring-8 Center, Sayo, Hyogo, 679-5148, Japan.

<sup>&</sup>lt;sup>r</sup> Japan Synchrotron Radiation Research Institute, Hyogo, Japan.

 $<sup>^{</sup>s}$  School of Chemistry, University of Nottingham, Nottingham , United Kingdom.

<sup>&</sup>lt;sup>1</sup> J.R. Macdonald Laboratory, Department of Physics, Kansas State University, Manhattan, Kansas 66506, USA.

<sup>&</sup>lt;sup>u</sup> Department of Chemistry, Tohoku University, Sendai 980-8578, Japan.

V Department of Chemistry, University of California, Davis, California 95616, USA. E-mail: ruforbes@ucdavis.edu

 $<sup>\</sup>dagger$  Supplementary Information available: [details of any supplementary information available should be included here]. See DOI: 10.1039/cXCP00000x/

that are in good agreement with tabletop measurements reported in the literature <sup>19,22</sup>. Delay-dependent shifts in the KE distribution of low energy  $I^{n+}$  ions are observed in the case of 1-IP. These are rationalised by assuming differing gradients for the potential energy surfaces involved in the neutral photodissociation and in the ionic states populated following probing. The experiment provides sensitive information about which CT processes can occur if the system is promoted to a high charge state whilst in the act of photodissociating, and about the dependence of these processes on the C-I separation and the initial iodine charge state. Small differences in this CT behaviour between the two isomers are observed. Finally, the sensitivity of this experiment to the recently proposed ultrafast HI elimination channel <sup>22</sup> is explored. Detailed analysis of the experimentally observed I<sup>+</sup> signal shows features that are consistent with ultrafast HI elimination in 2-IP. Such signal is not detected, within experimental uncertainty, in 1-IP.

#### 2 Methods

Experiments were performed at the soft X-ray FEL (BL1) beamline at the SACLA facility, using an ion imaging spectrometer  $^{38}$  in an experimental configuration similar to that described in other recent publications  $^{37-41}$ . To induce multiple ionization selectively at the I 4d site, the FEL photon energy was tuned to 95 eV, approximately in the centre of the I 4d giant dipole resonance, where the I 4d photoionization cross section is  $\sim\!20\text{--}30\,\text{Mb}^{42,43}$ . The 95 eV pulses, with estimated duration of 30 fs, were generated at 60 Hz and focused to a spot size of  $\sim\!10\,\mu\text{m}$  (1/e²) to the centre of the spectrometer using Kirkpatrick–Baez mirrors. The mean pulse energy, as measured by an upstream gas detector, was approximately 30  $\mu\text{J}$ , although the pulses were attenuated using a 650 nm thick Zr filter prior to their delivery to the endstation. Accounting for transmission through the filter, and expected beamline losses, the estimated mean on-target pulse energy was  $\sim\!3\,\mu\text{J}$ .

Ultraviolet pulses with a central wavelength of  $\sim\!\!267\,\mathrm{nm}$  were generated by frequency-tripling the 800 nm output of the BL1 optical Ti:Sapphire femtosecond laser  $^{44}$ . Before generating the third harmonic, the fundamental pulses were attenuated using a computer-controlled variable neutral density filter to generate UV pulses of a desired pulse energy (5  $\mu\mathrm{J}$  in the current experiments). The 267 nm light was focused into the interaction region of the spectrometer using a 2 m focal length lens, and was spatially overlapped with the FEL beam in a nearly colinear geometry. The delay of the optical laser relative to the FEL was controlled using a motorized delay stage. The single-shot jitter of the two pulses was measured using an arrival time monitor  $^{45}$ , and was used to correct and re-bin the data according to its true jitter-compensated delay.

The spectrometer used has been employed in several recent experiments at SACLA's BL1, and has been described in detail previously <sup>38</sup>. 1- and 2-IP were introduced to the spectrometer by expansion of their room temperature vapor pressure through a pulsed General Valve. The beam was collimated through a skimmer, before interaction with the focused UV and XUV beams. The ions were accelerated by a set of ion optics operating in VMI conditions <sup>46</sup> to a position- and time-sensitive detector, comprising dual-stacked microchannel plates and a hexanode delay line. The

detected positions of individual hits were reconstructed, and, in conjunction with their arrival times, used to determine the three-dimensional momentum of each ion. This calibration was performed using the output of ion trajectory simulations of the spectrometer. The data for the two molecules were recorded within a single few-day beamtime, with consistent experimental conditions between the two datasets.

# 3 Results and Discussion

#### 3.1 Probing UV induced C-I bond fission

Figure 1 presents the ion momentum distributions for the multiply charged ions from both 1-IP and 2-IP, as a function of pumpprobe time delay  $\tau$ . Here, a subtraction of averaged UV late data (-300 fs  $< \tau <$  -100fs) to remove contributions from XUV-only signal. Equivalent plots without this background subtraction are presented in the ESI (Fig. S1)<sup>†</sup>. Note, the production of some  $I^{n+}$  ions with n > 3, implies that the probe laser intensity in the present experiment was sufficient to support the absorption of multiple probe photons, as the total ionization energy for I<sup>4+</sup> ( $\sim$ 106 eV<sup>47</sup>) exceeds the probe photon energy. The I<sup>3+</sup> ion is excluded due to some overlapping contributions from the C<sub>3</sub>H<sub>7</sub><sup>+</sup> ion, which has a very similar mass-to-charge ratio (42.3 for I<sup>3+</sup>, 43 for C<sub>3</sub>H<sub>7</sub><sup>+</sup>). Delay-dependent signals are primarily observed in multiply charged iodine ions, as I 4d ionization followed by Auger-Meitner (AM) decay yields multiply charged species. As in our previous study of 2-IP<sup>37</sup>, clear pump-probe features are observed in the momentum distributions of multiply charged ions produced from either structural isomer. Three features dependent upon UV-induced C-I bond fission are identified (as labelled in Fig. 1, consistent with our previous work<sup>37</sup>):

I: Site-selective XUV multiple ionization at a dissociating iodine atom to produce  $\mathrm{I}^{(n+1)+}$  ions, followed by CT to the neutral propyl cofragment to yield  $\mathrm{I}^{n+}$  and  $\mathrm{C}_3\mathrm{H}_7^+$  (and potentially any smaller fragments derived therefrom) which Coulombically repel.

II: Site-selective XUV ionization at the departing iodine atom without subsequent CT, yielding low momentum multiply charged iodine ions whose momenta report on the UV photodissociation process.

III: XUV ionization of both the separating iodine and propyl fragments, producing a multiply charged iodine ion which repels against the charged partner fragments. The momenta of these ions are inversely related to the internuclear separation at the point of XUV ionization, and thus decrease with increasing pump-probe delay (forming a so-called 'Coulomb curve').

The delay-dependent behaviour of the momentum distribution associated with Channel II appears to differ between the two isomers. In the case of 2-IP, the momentum of this feature is essentially independent of the pump-probe delay, as observed in previous studies of other haloalkanes <sup>12,31,34,35</sup>). In 1-IP, the Channel II feature shows a shift to higher momentum over the first few hundred fs after time-zero. This trend is observable for multiple

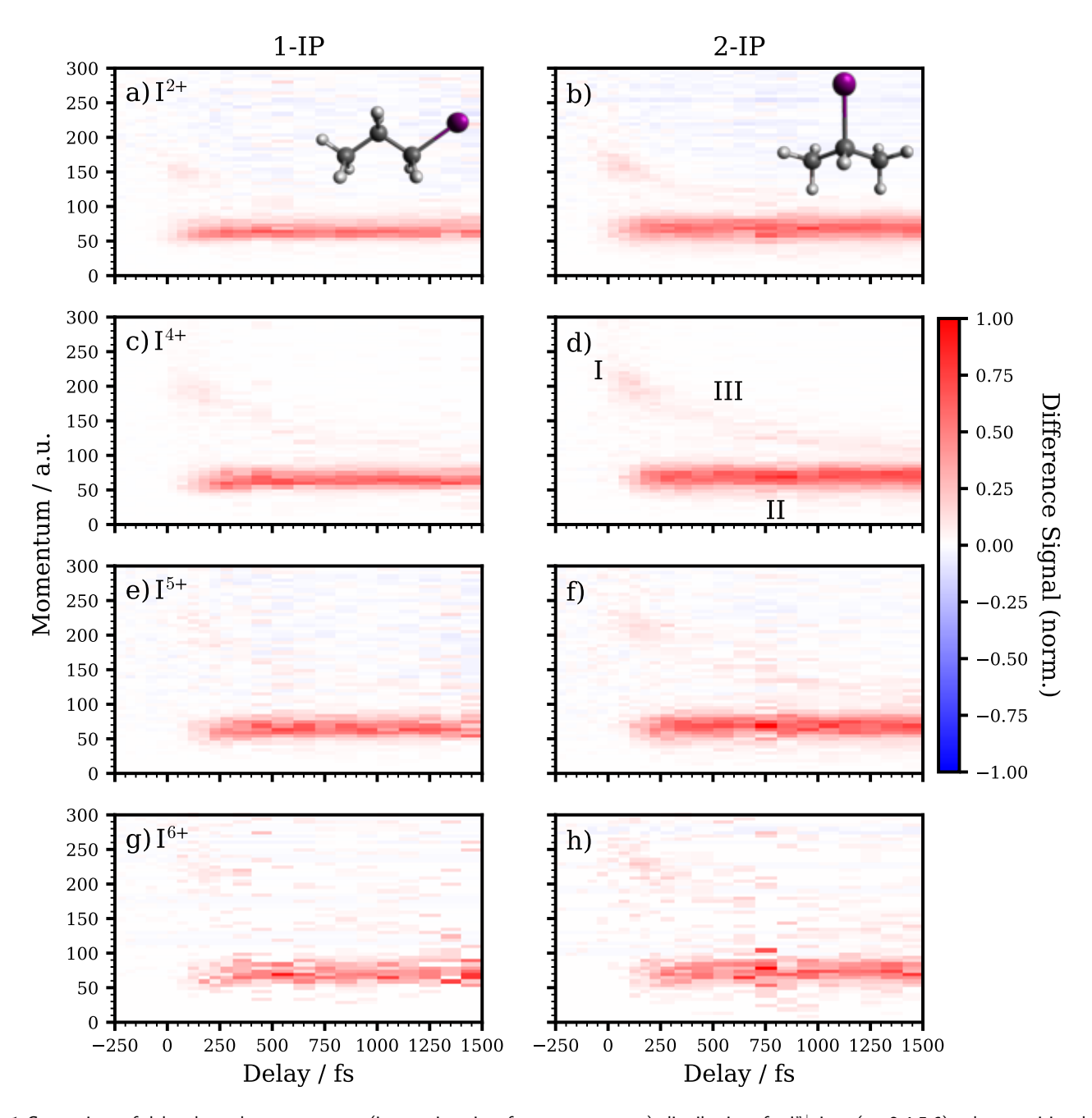


Fig. 1 Comparison of delay-dependent momentum (in atomic units of momentum, a.u.) distributions for  $I^{n+}$  ions (n=2,4,5,6), where positive delays corresponds to the UV pump arriving before the XUV probe, and vice versa. These data are presented following a subtraction of averaged UV late data (-300 fs to -100 fs), with red and blue colours representing relative enhancement and depletion, respectively. Data for each charge state are plotted on individually-normalised colour scales.

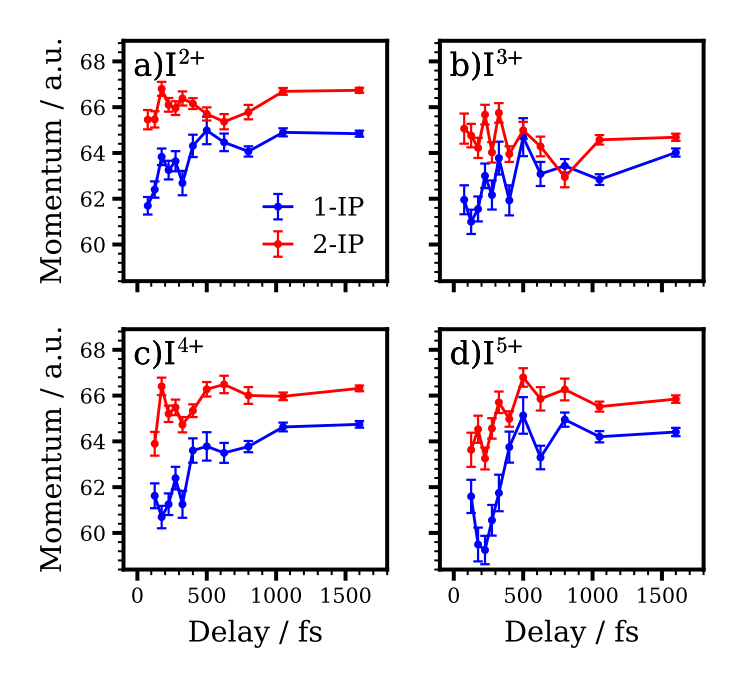


Fig. 2 Delay-dependent centre-of-mass momenta associated with Channel II as a function of pump-probe delay for 1-IP (blue) and 2-IP (red) for a)  $I^{2+}$ , b)  $I^{3+}$ , c)  $I^{4+}$ , d)  $I^{5+}$ .  $1\sigma$  error bars are shown assuming Poissonian counting statistics.

charge states. To explore this further, Figure 2 shows the mean momentum of the Channel II feature as a function of pump-probe delay. This is calculated by integrating the momentum distribution for the delay region, subtracting off an averaged UV-late background (averaged over -300 fs to -100 fs), and calculating the centre-of-mass (i.e. the mean) of the resultant distribution (for momenta, p<100 a.u.). For each charge state, this centreof-mass momentum is plotted for delays at which the Channel II signal in a given  $I^{n+}$  charge state has risen to at least 25% of its asymptotic value. I<sup>6+</sup> is excluded from this analysis due to poor signal-to-noise ratio when the data is partitioned into fine pumpprobe delay bins. The  $I^{3+}$  ion is included in this analysis as the low momentum Channel II ions were suitably localized in timeof-flight to not overlap with the C<sub>3</sub>H<sub>7</sub><sup>+</sup> ion. Alternative representations of these delay-dependent Channel II momenta are presented in the ESI (Figs. S2 and S3)†. For 1-IP, the mean momentum at the shortest delays is 62 a.u., rising to its asymptotic value of  $\sim$ 64 a.u. on a few hundred fs timescale. For 2-IP, any delaydependence is much less pronounced and difficult to distinguish above the uncertainty of the measurement. The delay-dependent changes observed in 1-IP appear to be roughly consistent across the different  $I^{n+}$  charge states.

In principle, one can envisage several reasons why the momenta of ions produced via Channel II might vary as a function of pump-probe delay. If the timescale for dissociations yielding products with different recoil velocities varied significantly (e.g. because of multiple dissociation channels with different lifetimes <sup>41</sup>), this could lead to delay-dependent momenta for Channel II ions. Given the expected purely repulsive nature of the excited-state potentials involved in both the I and I\* product channels <sup>19</sup>, however, we do not expect substantially different

dissociation timescales associated with different recoil velocities.

The specifics of the probing mechanism must also be considered, namely multiple XUV-induced ionization of the dissociating I fragment, without CT to the partner propyl radical. Within the OTB model, CT is probable up until some fixed critical distance, determined by the charge state of the accepting iodine ion and the ionization potential of the cofragment. For a fixed critical distance, one would expect that dissociations with a higher recoil velocity would exceed the critical distance at earlier delays. However, this would result in a small shift to higher ion momentum at the earliest pump-probe delays, the opposite trend to that observed experimentally. It should be noted that the impact of this effect in reality is lessened by CT probability and internuclear distance having a more complex and gradual relationship than the sharp cutoff implied by the OTB model<sup>37</sup>. We would also expect such an effect to be in operation (with similar magnitude) for both isomers.

Another possibility is that the precise delay at which the system is probed affects the measured momenta of the  $I^{n+}$  ions directly. Prior to probing, the neutral I/I\* is separating from its C<sub>3</sub>H<sub>7</sub> partner on the relevant neutral dissociative Potential Energy Surface(s) (PES(s)). After probing (I 4d core ionization(s) and AM decay(s)), this motion continues along different PESs correlating to  $I^{n+}$  and neutral (presumably intact)  $C_3H_7$  products. If probing happens prior to the system having accelerated to the asymptotic neutral fragment velocities, the final velocity of the  $I^{n+}$  ion will be additionally influenced by the topography of the PES of the polycation. The observed overall trend in the 1-IP data could be understood if the relevant long-range parts of the various polycation PESs were generally shallower than that of the excited-state neutral; earlier probe times would then correspond to the system spending more time on the shallower potential, and accelerating to a lower asymptotic momentum. It should be emphasized that the PES is multidimensional, and so so the regions of the PES sampled as a function of delay depend on the rovibrational motion of the C<sub>3</sub>H<sub>7</sub> fragment at the early stages of the

Qualitatively similar behaviour was noted in a previous study on CH<sub>3</sub>I<sup>6</sup>, in which the molecule was photoexcited within the A-band, prior to non-resonant multiphoton single ionization by an 800 nm probe pulse. On a timescale of several hundred fs, the KEs of the detected  $CH_3^+$  ions were observed to increase by  $\sim 10\%$ . The observation was ascribed to the cationic final state having a flatter potential along the dissociation coordinate than the neutral states involved in the photodissociation. If this is the origin of the observed isomer-selective, delay-dependent ion momenta, it is interesting that such an effect is much more prominent in 1-IP than 2-IP. Any full exploration of this effect would likely involve theoretical characterization of both the neutral excited-state PESs populated following photoexcitation and the ionic PESs populated following inner-shell ionization and AM decay. Such calculations are out of the scope of the current work but could be very illuminating. We also note that qualitatively similar effects have been seen in other pump-probe experiments, in addition to the aforementioned study on CH<sub>3</sub>I probed by multi-photon single ionization<sup>6</sup>. For instance, a UV pump - NIR probe time-resolved

Coulomb explosion imaging study of CH<sub>3</sub>I observed an immediate rise in product KEs close to time-zero due to the dication surfaces involved in the probing having a shallow potential well close to the vertical Franck-Condon region<sup>48</sup>. A UV pump - VUV probe time-resolved ion imaging study of CH<sub>2</sub>I<sub>2</sub> and CH<sub>2</sub>IBr dissociation also observed delay-dependent ion momentum distributions which were attributed to relatively flat potentials in the cationic states accessed in the probe step <sup>49</sup>.

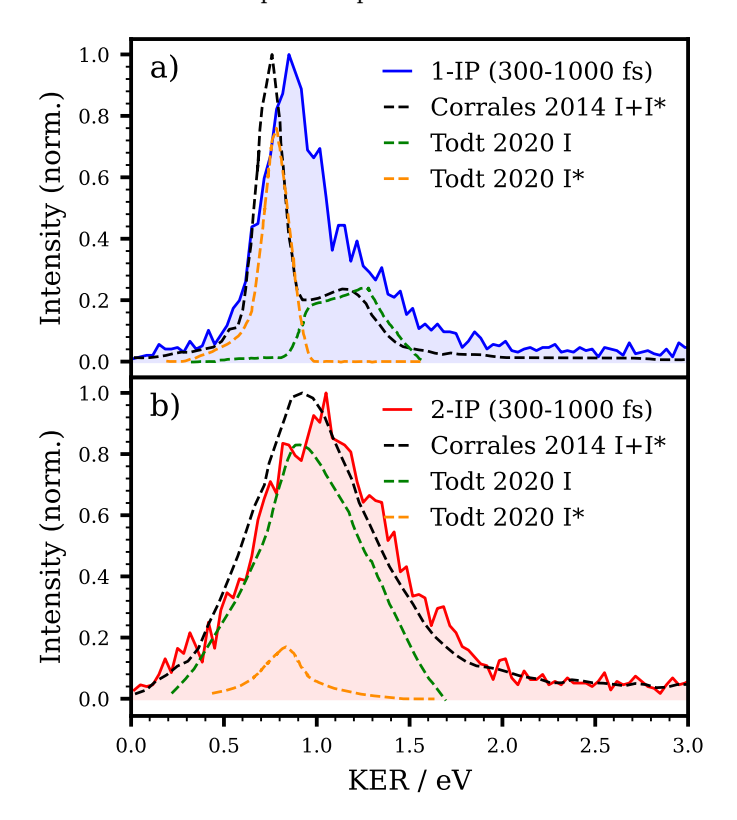


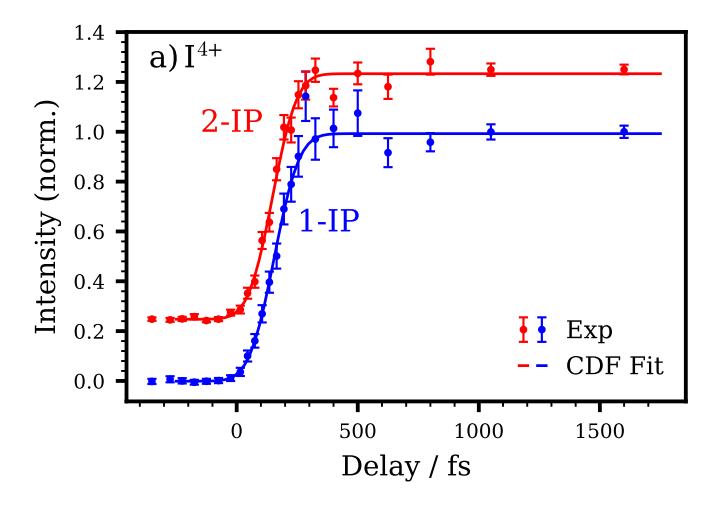
Fig. 3 KER distributions associated with Channel II for the  $\rm I^{4+}$  ion for both 1-IP and 2-IP, obtained by integrating the background-subtracted momentum distributions over the pump-probe delay range shown. This is compared to previously reported KER distributions for the neutral photodissociation of 1-IP and 2-IP at around 266 nm  $\rm ^{19,22}$ , as described in detail in the main text.

Figure 3 displays the long time (300<  $\tau$  <=1000 fs) total kinetic energy release (KER) distributions associated with Channel II for both 1-IP and 2-IP, assuming a C<sub>3</sub>H<sub>7</sub> co-fragment. These are derived from the I<sup>4+</sup> ion, although very similar distributions are seen across all the observed charge states (shown in Fig. S4 of the ESI<sup>†</sup>). These two distributions are compared to two prior measurements <sup>19,22</sup>. Corrales et al. <sup>19</sup> photoexcited the molecules with a femtosecond pump pulse, and monitored both the I and I\* products by (2+1) resonance-enhanced multiple photon ionization (REMPI) at 304.5 nm with a femtosecond probe pulse. Todt et al. 22 photoexcited with a nanosecond 266 nm laser pulse. The I\* photoproducts were probed by a (1+1') REMPI process, with the intermediate state populated by a 128.94 nm laser pulse. I\* (and HI, as discussed in Section 3.3) photoproducts were ionized with a single photon at around 125 nm. This corresponds to a 9.9 eV photon energy, lying above the ionization potential of I\*, but below that of ground-state iodine atoms. To enable comparison between the literature distributions and those reported in the current work, each is normalized to their maximum intensity. For the spin-orbit resolved measurements of Todt et al., these are then re-scaled by the I:I\* branching ratios reported in that work, which are 0.24:0.76 and 0.83:0.17 for 1-IP and 2-IP, respectively. The presently-reported asymptotic KER distributions agree well with the literature data. The current distributions are slightly broader than the literature data, consistent with a poorer energy resolution in the present work. This is in part due to the specifics of the spectrometer, which is optimized for imaging much highervelocity ions resulting from Coulomb explosions<sup>38</sup>. Relative to the prior studies, the present data for 1-IP also hint at a larger than expected contribution from the minor I atom product channel (appearing as a high-KE shoulder). This could imply that the ground-state I atom has a higher I 4d photoabsorption than I\* atoms at the present (95 eV) photon energy, though we are not aware of any previous spin-orbit resolved cross-section measurements. For both isomers, the present measurements peak at slightly higher KER values than the literature measurements. For 1-IP, this may just be a consequence of the limited energy resolution, which results in greater overlap between the I and I\* channels. For 2-IP, some shift to higher KERs would be expected if overlapping signal from Coulomb explosion of photoeliminated HI was present, which is discussed in detail in Section 3.3. Some small error may also arise in the calibration of the spectrometer's magnification, which is determined by particle trajectory simulations and therefore can present slight errors if the ions are born in a slightly different region of the spectrometer than that assumed in the simulation.

#### 3.2 Charge transfer processes

Figure 4a) shows the delay-dependence of the I<sup>4+</sup> Channel II yields from both molecules along with best-fits using a normal cumulative distribution function (CDF) as employed in prior work  $^{27,30-32}$ . The appearance of Channel II ions is associated with the cessation of CT. Consequently, the time at which Channel II intensity is expected should vary with I<sup>n+</sup> charge state. Delay-dependent Channel II yields for all I<sup>n+</sup> charge states are presented in the ESI, with their corresponding CDF fits (Fig. S5)<sup>†</sup>.

Figure 4b) shows the centre of CDF fits to the delay-dependent ion yields across charge states in both isomers. The I<sup>3+</sup> ion could be included in this analysis as the low momentum Channel II ions were suitably localized in time-of-flight to not overlap with the C<sub>3</sub>H<sub>7</sub><sup>+</sup> ion. A shift to later delays for higher charge states is observed in both 1-IP and 2-IP, confirming the expectation that CT can occur over greater distances and thus out to longer pumpprobe delays for higher charge states. For both molecules, these delays are plotted relative to that of the I<sup>2+</sup> ion. This negates the effects of any small undetected drifts in time-zero between the two measurements, and any error in the precise assignment of time-zero, as was done in a prior work 12. Generally, the shift to longer pump-probe delays with increasing charge state is greater in 1-IP than 2-IP (with the exception of the I<sup>6+</sup> ion, although in both datasets the error of this value is relatively large due to the weak signal in this channel). Within the approximations of the



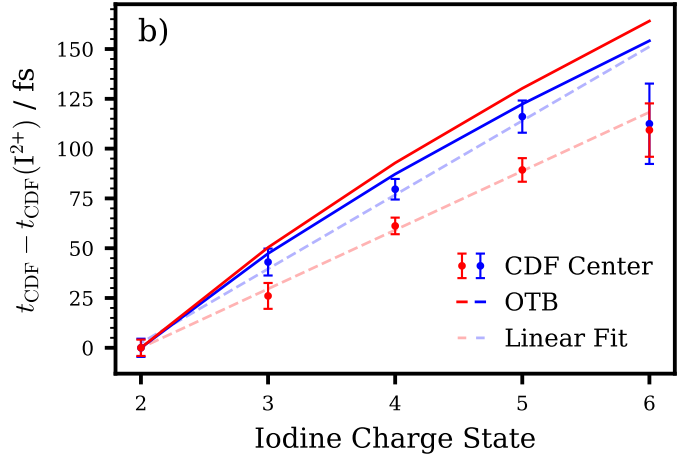


Fig. 4 a) Delay-dependent yields of the Channel II ions for  $I^{4+}$  ions in 1-IP (blue) and 2-IP (red). These are normalized by their maximum value, and are vertically offset for clarity. Fits to a normal CDF are also shown. b) Comparison of the centre of the CDF fits (circles with error bars representing statistical error from the CDF fit) as a function of iodine charge state for 1-IP (blue) and 2-IP (red). As described in the main text, these were referenced relative to the observed centre for the  $I^{2+}$  ion. Linear fits to these data are shown to guide the eye (dashed lines). Comparison is also drawn to predictions from the OTB model for the two species (solid lines, see text for more details).

OTB model, assuming a constant recoil velocity following photoexcitation (and neglecting the role of any rotational/vibrational motion of the alkyl fragment), critical distances can be converted into critical pump-probe delays, as shown by the solid lines in Fig. 4b. As discussed previously Due to the very similar mean photodissociation velocity of the two isomers, 1-IP and 2-IP are predicted to behave almost identically. The observed differences between the isomers may arise from structural/dynamical influences on CT which are not captured by the OTB model since it treats both propyl radicals and cations as unstructured point charges. The 1- and 2-propyl radicals produced following photo dissociation of the two isomers are distinct, and also undergo substantially different nuclear motion. In 1-IP, the large torque imparted by the photodissociation results in substantial rotational excitation of the radical, while in 2-IP, the nuclear dynamics of the radical are dominated by 'umbrella-like' vibrational motion as a result of the impulse imparted to the central C atom as the C–I bond extends  $^{19,22}$ . The possible influence of rotational motion on the cessation time for CT has also been considered in a previous study of CH<sub>2</sub>BrI, where the recoiling CH<sub>2</sub>Br fragment formed following C–I bond fission was deduced to carry substantial rotational excitation<sup>34</sup>. In 1- and 2-IP, we might expect that rovibrational motion following dissociation would affect the delay-dependent distance between the  $I^{n+}$  ion and the molecular orbital (presumably the singly-occupied molecular orbital) of the  $C_3H_7$  radical from which electron donation occurs. It is, however, unclear quantitatively how such effects might influence the data shown in Figure 4.

Our previous work focused on the high momentum  $I^{n+}$ ions produced from CT immediately after time-zero in 2-IP molecules <sup>37</sup> (i.e. the Channel I signal), the precise momenta of which could be related to the separation between the charged iodine atom and the neutral C<sub>3</sub>H<sub>7</sub> partner at the instant of CT. As shown in Fig S7 of the  $\mathrm{ESI}^\dagger$ , the momentum distributions derived from this feature for a given charge state are essentially isomer independent, implying very similar Coulombic repulsions at the point of CT within photodissociating 1- and 2-IP molecules. The only exception to this is in the I<sup>2+</sup> ion, which appears to be produced with a slightly higher KER in 2-IP. 2-propyl radicals have a lower ionization potential than 1-propyl radicals (7.47 eV, cf. 8.09 eV<sup>50</sup>). The OTB model would thus predict slightly ( $\sim$ 0.6-1) longer critical distances in 2-IP. Several factors could account for our non-observation of such a shift, such as approximations inherent in the OTB model, the aforementioned differences in the structure and dynamics of the recoiling propyl radicals, and differences in the charge distributions within the 1- and 2-propyl cations (which determine the Coulombic repulsion felt by the  $I^{n+}$ ion). A similar shift might be expected in the delay-dependent intensities of Channel II ions, but the expected magnitudes of any isomer-dependent shifts ( $\sim$ 20-30 fs) are less than the uncertainty in the assignment of time-zero, which may differ between the two datasets. We also note that theoretical work suggests that the  $C_3H_7^+$  ion has two stable structures: the 2-propyl structure and a protonated cyclopropane structure <sup>51</sup>. From the current data, we cannot comment on whether the suspected unstable nature of the 1-propyl C<sub>3</sub>H<sub>7</sub><sup>+</sup> structure affects the experimental signal for Channels I or II from 1-IP, but this would be interesting to explore in future work.

## 3.3 Probing UV induced HI elimination

As mentioned previously, Todt *et al.* reported detection of HI molecules eliminated from UV photoexcited 2-IP molecules <sup>22</sup>. Based on measurements of the strongly-anisotropic recoil velocity of these products, it was concluded that HI formation occurred on ultrafast (few hundred fs) timescales, as dissociation must occur prior to significant rotation of the parent molecule, which would lead to a more isotropic angular distribution. In contrast, no such signal was observed following UV excitation of 1-IP. These results were broadly in agreement with a prior report by Ross and Johnston <sup>26</sup>, who observed signatures of HI elimination following 248 nm photoexcitation of 2-IP but not 1-IP in a study involving

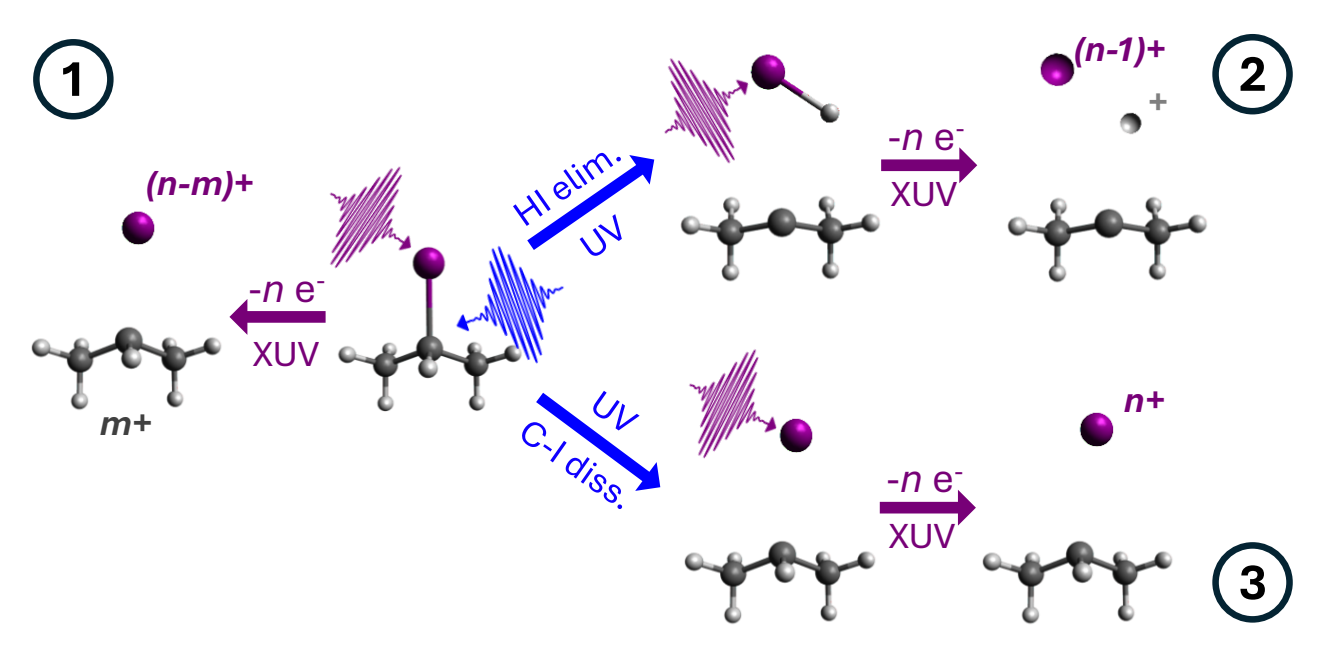


Fig. 5 Schematic of different processes relevant to ultrafast HI elimination. Process 1: XUV-only multiple ionization of the molecule to yield parent in n+ charge state, that Coulomb explodes into  $I^{(n-m)+}$  and  $C_3H_7^{m+}$  (or smaller derived fragments). Process 2: UV-induced HI elimination, followed by XUV multiple ionization of HI to HI $^{n+}$  that Coulomb explodes into  $I^{(n-1)+}$  and H $^+$ . Process 3: UV-induced C–I bond cleavage, following by XUV multiple ionization of the atomic I product to  $I^{n+}$ .

a range of iodoalkanes. Todt  $et\ al.^{22}$  also showed that the HI photoproducts from 2-IP were produced with a very similar KER distribution to that of the ground-state I atoms from the C–I bond dissociation channel.

Figure 5 schematically depicts the potential impact of HI elimination on the signals observed in the present work, focusing on channels that are expected to contribute significantly (i.e. ignoring single valence ionization of HI by the probe pulse, which has a substantially lower cross-section than I 4d ionization), and ignoring CT processes that occur at very early pump-probe delays. Specifically, UV-induced HI elimination followed by I 4d ionization(s) of the neutral HI products will yield multiply charged  $HI^{n+}$ , which will Coulomb explode into  $H^+ + I^{(n-1)+}$  (Process 2 in Figure 5). The momenta of the  $I^{(n-1)+}$  ions produced will have two contributions, from the HI elimination and the  $HI^{n+}$ Coulomb explosion, respectively. Whilst the KER associated with the second step will be much greater, the impulse imparted to the iodine is rather small, due to the very large discrepancy between the masses of iodine (127 Da) and hydrogen (1 Da). As explored quantitatively shortly, this means that the associated  $I^{(n-1)+}$  momentum distribution would largely reflect that of the HI elimination step, albeit broadened and shifted slightly to higher values. Consequently, such  $I^{(n-1)+}$  signal overlaps heavily with that arising from UV-induced C-I cleavage followed by I 4d ionization (Process 3 in Figure 5). However, Process 3 only contributed negligible signal to the I<sup>+</sup> ion, as I 4d ionization deposits multiple charges on the atom and the expected cross-section for valence ionization is almost two orders of magnitude lower 42,43. Therefore, the I+ ion, which can be produced through Process 2 but not Process 3, is expected to show the highest sensitivity to any ultrafast UV-induced HI elimination.

Figure 6 presents the delay-dependent momentum distribu-

tions for the I+ ion, shown with and without subtraction of the averaged UV-late signal. At all pump-probe delays, the signal of both isomers is dominated by high momentum signals (centred at  $\sim$ 140 a.u.), which arise from various XUV-induced Coulomb explosion channels of the unpumped molecule which yield I<sup>+</sup> together with a charged partner or partners (Process 1 in Figure 5) <sup>39,40</sup>. As can be seen better in the subtracted data, this I<sup>+</sup> signal is depleted shortly after time-zero, indicating some reduction in the number density of intact parent molecules (due to UV induced excitation/dissociation). However, no obvious enhancement of signal at lower momenta due to Process 2 is observed in either case. This may not be surprising given that the I<sup>+</sup> ion yield is dominated by broad probe-only signal, and the branching ratio of the HI elimination channel following photoexcitation of 2-IP is small ( $\sim$ 10%<sup>22</sup>). Consequently, any additional signal arising from Process 2 may well be 'masked' by depletion of the low-momentum tail of the distribution associated with Process 1. Panels e) and f) compare the I<sup>+</sup> momentum distributions from 1-IP and 2-IP, integrated over all UV-late (magenta) and UV-early (green) pump-probe delays. The averaged percentage difference is shown in orange. For both isomers, a depletion is seen across a wide momentum range. For 2-IP, however, the extent of depletion decreases at low momentum (p $<\sim$  100 a.u.), and, within the error bounds, no I<sup>+</sup> signal depletion is observed for p $<\sim$ 60 a.u. This could indicate a (small) enhancement in the case of 2-IP in this low p region, sitting on top of the broad depletion of XUVonly signal. We also note here that the overall depletion is significantly greater in 2-IP than 1-IP, despite both datasets using the same nominal UV fluence. This is consistent with the respective UV photoabsorption cross-sections: 1.20 Mb for 2-IP, cf. 0.82 Mb for 1-IP at 270 nm 15.

To analyse the delay-dependent I<sup>+</sup> data more quantitatively,

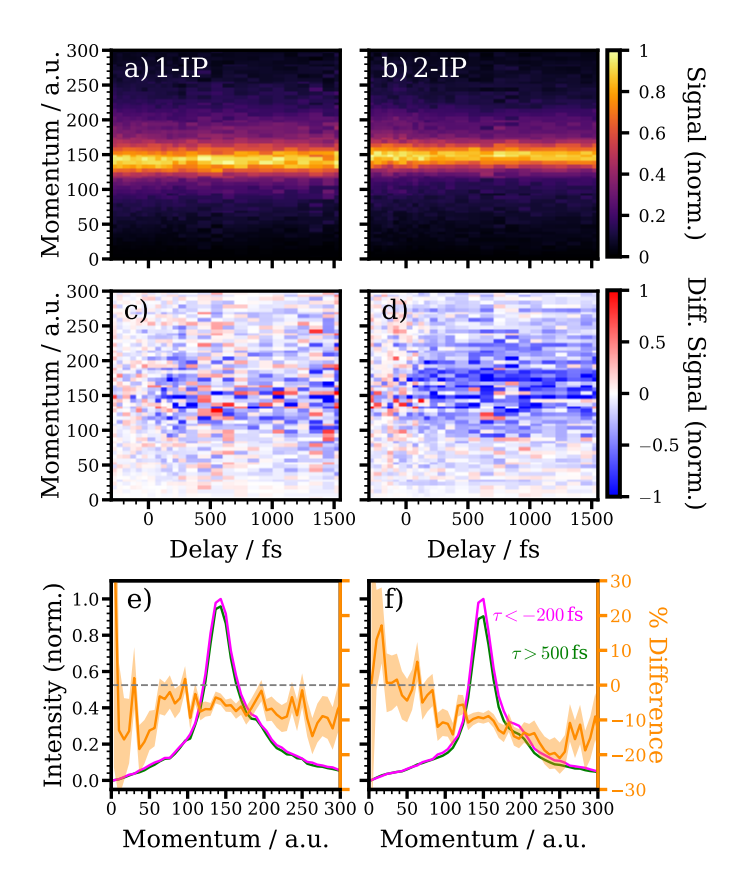


Fig. 6 Delay-dependent I<sup>+</sup> momentum distribution for 1-IP (a) and c)) and 2-IP (b) and d)). These distributions have been normalized by the averaged FEL pulse energy per delay bin. Panels c) and d) present the same data following subtraction of an averaged UV-late contribution. Panels e) and f) compare momentum distributions integrated over all UV late (magenta) and UV early delays (green) for the two isomers. Percentage difference signals (of UV early relative to UV late), with shaded  $1\sigma$  uncertainties are presented in orange.

Figures 7a) and b) compare I<sup>+</sup> momentum distributions arising via Process 1 and 2 for 1-IP and 2-IP. For Process 1, this is measured directly in the experiment in the UV-late pump-probe delays. To predict the expected Process 2 signal, we sampled the HI momenta reported previously from UV excitation of 2-IP<sup>22</sup>, and simulated the Coulomb explosion of the resultant HI into H<sup>+</sup> and I+ ions. The KER of the Coulomb explosion process was sampled from a Gaussian distribution with mean 6 eV and standard deviation 0.5 eV. Assuming purely classically Coulombic forces in the explosion, 6 eV KER would correspond to a I-H internuclear separation of  $\sim$ 2.4 Å. This value was chosen to be longer than the 1.6 Å equilibrium internuclear distance, to allow for any decrease in KER due to factors such as I-H bond extension during the explosion, vibrational excitation of the nascent HI products, and deviations from Coulombic behaviour in the PESs governing the explosion. We note that the precise KE of the I<sup>+</sup> products from Coulomb explosion of the HI is not critical in the analysis, as demonstrated in the ESI<sup>†</sup>. It was assumed that there is no angular correlation between the recoil velocity of the eliminated HI product and that of the Coulomb explosion. No clear HI signal from UV photolysis of 1-IP has been reported previously <sup>22,26</sup>, but, for consistency, we also sought to simulate how any such HI products from photoexcited 1-IP might contribute to the data shown in Figs. 6 and 7. In the case of 1-IP, our modelling assumed that the KER distribution of any HI products resembled that of the I atom products. Similar results were produced assuming the KER distribution of any HI products instead resembled that of the I\* atoms, as shown in the ESI $^\dagger$ . In both cases, the I $^+$  signal from Process 2 overlaps heavily with the low-momentum tail of that arising from Process 1.

We define momentum gates a (130 a.u.p<300 a.u.) and b (40 a.u. $\leq p \leq 90$  a.u.) which capture the majority of the momenta distributions associated with Processes 1 and 2 respectively. The ratio of the experimental signal within these regions as a function of pump-probe delay is plotted in Figure 7c), for both 1-IP and 2-IP. In the case of 1-IP, no clear change in this ratio with pump-probe delay is observed, which would be expected if only Process 1 contributes to the I<sup>+</sup> signal at all pump-probe delays. In 2-IP, however, this ratio shows a noisy step at pump-probe delays close to time-zero, with relatively more signal in momentum gate b (associated with Process 2, Coulomb explosion of HI) measured when the UV pulse precedes the XUV pulse. This can also be seen clearly by averaging data which is before ( $\tau < -200 \, \mathrm{fs}$ ) and significantly after ( $\tau > 500 \, \text{fs}$ ) time-zero, which are shown by the shaded horizontal bands Figure 7c). These data are entirely consistent with what would be expected from an ultrafast HI elimination process that is much more prominent in 2-IP than 1-IP, as suggested by Todt et al. 22. With the limited signal-to-noise ratio of the current data, it is not possible to quantify the timescale of the change in this ratio accurately, but based on the data shown in Figure 7c), we conclude that this happens on a sub-ps timescale.

If we assume that XUV probing of HI or  $C_3H_7I$  yields  $I^+$  with equal propensity, and that photoexcitation necessarily leads to either prompt C–I bond cleavage or HI elimination, (i.e. prevents Process 1), the ratio of ions in momentum gate b, n(b) to those in gate a, n(a) following UV excitation can be written as:

$$\frac{n(b)}{n(a)} = \frac{b_{P1} \times (1 - \theta) + b_{P2} \times \theta \Phi}{a_{P1} \times (1 - \theta) + a_{P2} \times \theta \Phi}$$
(1)

where  $a_{Pi}$  and  $b_{Pi}$  are the fraction of the I<sup>+</sup> momentum distributions for Process i (i = 1 or 2) within ion momentum gates aand b.  $\theta$  is the UV excitation fraction and  $\Phi$  is the branching ratio for HI elimination. As  $a_{P2} = 0$  for the chosen momentum gates (i.e. no signal from HI CE is expected to contributed to the higher momentum region),  $\theta$  can be determined from the ratio of n(b) before and after time-zero, which yields excitation fractions of  $6.3\pm0.6\%$  and  $12.3\pm0.6\%$  for the 1-IP and 2-IP data, respectively. Taking the value of  $\frac{n(b)}{n(a)}$  averaged for UV early data then gives the branching ratios for HI elimination,  $\Phi$ , of  $1\pm2\%$  and  $6\pm1\%$  for 1-IP and 2-IP, respectively. These values are in good general agreement with those reported by Todt et al., <0.21% for 1-IP and 10.5% for 2-IP. Both suggest negligible UV-induced HI elimination from 1-IP, but that HI is a primary (albeit minor) photoproduct following UV photolysis of 2-IP. We attach little weight to the lower (absolute) value of the branching into HI products from 2-IP determined in the current work, given systematic errors in our analysis which are challenging to assess quantitatively. These stem from various assumptions made in the analysis, which

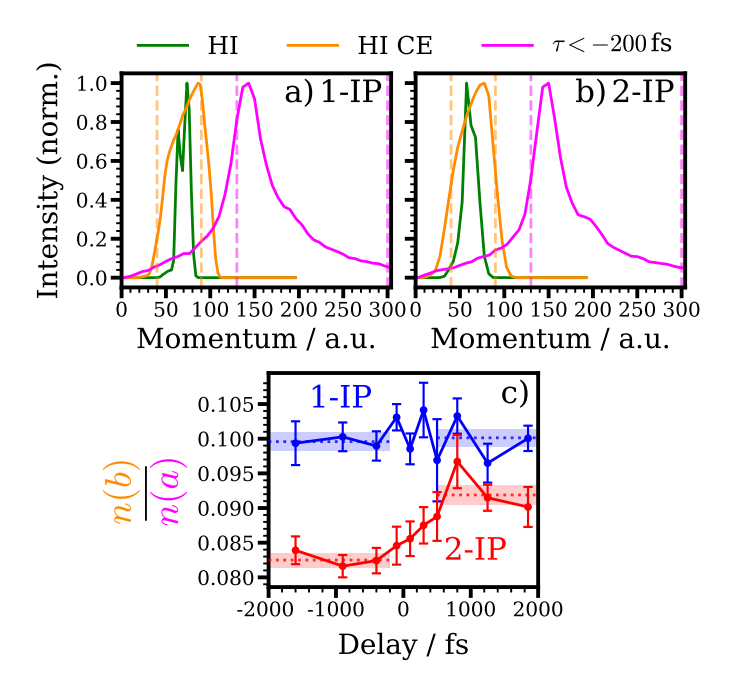


Fig. 7 Momentum distributions relevant to the analysis of the delay-dependent I+ signals in 1-IP (a) and 2-IP (b), showing the expected momentum distribution for HI elimination (green), the simulated I+ momentum distribution for Coulomb explosion of eliminated HI (orange), and the experimental I+ momentum distribution averaged over UV-late pump-probe delays (magenta). The derivation of assumed HI product momentum distributions is described in the main text. The momentum regions a and b, described in the main text, are indicated by the dashed orange and magenta lines. Panel c) shows the delay-dependent ratio of ions observed in the two momentum regions as a function of pump-probe delay for 1-IP (blue) and 2-IP (red). Averaged values for UV late  $(\tau < -200\,\mathrm{fs})$  and UV early  $(\tau > 500\,\mathrm{fs})$  are shown by the horizontal dotted lines.

are discussed in detail in the  $ESI^{\dagger}$ .

 ${
m H}^+$  ions could not be detected in the present work due to a significant scattered light signal which saturated the MCP/delay-line detector for early times-of-flight. Future work which examines correlations between  ${
m H}^+$  and  ${
m I}^+$  ions, ideally isolating signal from Process 2, could be very informative. The KER distribution associated with CE of the photoeliminated HI products could contain information about their vibrational state population distribution  $^{52,53}$ . If performed with suitably high resolution, these measurements could also be sensitive to any HI product rotation, as recently demonstrated for the  ${
m CH}_2{
m X}$  fragment formed by photoinduced C–I bond fission in dihalomethanes  $^{54}$ . Studies on larger, more branched iodoalkanes, such as t-butyl iodide, where the HI elimination channel has been suggested to be more prevalent  $^{22}$  would also be of interest.

#### Conclusions

The UV-induced photodynamics of the structural isomers 1- and 2-IP were studied in a time-resolved scheme incorporating site-selective XUV ionization above the I 4d edge as the probe. Consistent with prior work, the primary dynamics following excitation to the A band in both molecules are prompt dissociation to yield propyl radicals and I atoms, in both their ground and excited

spin-orbit states. In the case of 1-IP, delay-dependent shifts in the momenta of the  $I^{n+}$  ions produced by UV-induced C–I dissociation followed by multiple ionization are observed, which may be rationalised by invoking differences in the gradients of the relevant neutral and polycationic PESs along the dissociation coordinate. As observed in simpler haloalkanes, there is a systematic shift in the onset of this channel across charge states, which relates to the distance dependence of CT processes enabled following multiple ionization. Subtle differences in this behaviour between the two isomeric species were observed. Without more detailed modelling, the precise origin of this behaviour is difficult to assign, but may relate to the substantially different nuclear motion undergone by the recoiling propyl radical in the two systems. Finally, possible signals arising from the XUV-induced Coulomb explosion of photoeliminated HI were examined. A simple scheme was presented to model this potential process, which yields results that are consistent with observations for the 2-IP isomer. These results support the recent report 22 that ultrafast HI elimination is a minor channel in photoexcited 2-IP which is either absent, or much less prevalent, in the unbranched 1-IP isomer.

#### Author contributions

F. A. and R. F. conceived the experiment, the plan for which benefited from further input from J. H., R. M. and K. N. The sample delivery and spectrometer were prepared by J. H. and K. N., Y. K. arranged the data acquisition software and prepared and operated the detector. S.O. prepared the beamline along with the optical laser. The experiment was conducted onsite by J. H., H. I., Y. K. and K. N., with online participation in the experiment by all coauthors. The experiment data was analyzed by F. A. and Y. K. Finally, F. A., M. A. and R. F. interpreted the results and wrote the manuscript with input from all the authors.

# Conflicts of interest

There are no conflicts to declare.

# Data availability

A data availability statement (DAS) is required to be submitted alongside all articles. Please read our full guidance on data availability statements for more details and examples of suitable statements you can use.

# Acknowledgements

The experiment was performed at SACLA with the approval of JASRI and the program review committee (proposal No. 2021A8038 Forbes). We thank the technical and scientific staff of SACLA for their hospitality and support before and during the beamtime. We thank Luis Bañares and Jesús González-Vázquez for helpful discussions regarding the photodissociation dynamics of 1- and 2-IP. R.F. and F.A. gratefully acknowledge support from the Linac Coherent Light Source, SLAC National Accelerator Laboratory, which is supported by the US Department of Energy, Office of Science, Office of Basic Energy Sciences, under contract no. DE-AC02-76SF00515. Y.K. acknowledges support from JSPS KAKENHI Grant No. 20K14427. M.Bu., J.U., and T.W. are grateful to EPSRC for support from EP/S028617/1. T.W. is

additionally thankful to EPSRC for studentship funding and Jesus College, Oxford, for a partial fee scholarship. J.U. is also grateful to the States of Jersey for studentship funding. M.Br and J.W.M. are grateful to the EPSRC for support from Programme Grant EP/V026690/1. C.V., D.H., D.M. and P.R. are grateful to the EPSRC for support from Proamme Grants EP/V026690/1 and EP/T021675/1. D.R. was supported by the Chemical Sciences, Geosciences, and Biosciences Division, Office of Basic Energy Sciences, Office of Science, US Department of Energy (grant no. DE-FG02-86ER13491). RSM thanks the EPSRC(EP/X027635/1 and EP/R010609/1) and Leverhulme Trust (RPG-2021-257) for funding. B.D.W. thanks the CLF and the University of Southampton for a studentship. F.A. thanks the Alexander von Humboldt Foundation for their support.

## Notes and references

- 1 D. W. Chandler and P. L. Houston, *The Journal of Chemical Physics*, 1987, **87**, 1445–1447.
- 2 K. Q. Lao, M. D. Person, P. Xayariboun and L. J. Butler, *The Journal of Chemical Physics*, 1990, **92**, 823–841.
- 3 A. T. J. B. Eppink and D. H. Parker, *The Journal of Chemical Physics*, 1998, **109**, 4758–4767.
- 4 A. T. J. B. Eppink and D. H. Parker, *The Journal of Chemical Physics*, 1999, **110**, 832–844.
- 5 R. de Nalda, J. Durá, A. García-Vela, J. G. Izquierdo, J. González-Vázquez and L. Bañares, *The Journal of Chemical Physics*, 2008, **128**, 244309.
- 6 J. Durá, R. De Nalda, G. Amaral and L. Bañares, *The Journal of Chemical Physics*, 2009, **131**, 134311.
- 7 L. Rubio-Lago, A. García-Vela, A. Arregui, G. Amaral and L. Bañares, *The Journal of Chemical Physics*, 2009, 131, 174309.
- 8 A. Tehlar and H. J. Wörner, *Molecular Physics*, 2013, **111**, 2057–2067.
- 9 A. R. Attar, A. Bhattacherjee and S. R. Leone, *The Journal of Physical Chemistry Letters*, 2015, **6**, 5072–5077.
- 10 F. Allum, M. Burt, K. Amini, R. Boll, H. Köckert, P. K. Olshin, S. Bari, C. Bomme, F. Brauße, B. Cunha de Miranda et al., The Journal of Chemical Physics, 2018, 149, 204313.
- 11 M. Corrales, J. González-Vázquez, R. De Nalda and L. Bañares, *The Journal of Physical Chemistry Letters*, 2018, **10**, 138–143.
- 12 R. Forbes, F. Allum, S. Bari, R. Boll, K. Borne, M. Brouard, P. H. Bucksbaum, N. Ekanayake, B. Erk, A. J. Howard et al., Journal of Physics B: Atomic, Molecular and Optical Physics, 2020, 53, 224001.
- 13 K. F. Chang, H. Wang, S. M. Poullain, D. Prendergast, D. M. Neumark and S. R. Leone, *The Journal of Chemical Physics*, 2021, **154**, 234301.
- 14 M. L. Murillo-Sánchez, J. González-Vázquez, M. E. Corrales, R. de Nalda, E. Martínez-Núñez, A. García-Vela and L. Bañares, *The Journal of Chemical Physics*, 2020, 152, 014304.
- 15 C. M. Roehl, J. B. Burkholder, G. K. Moortgat, A. Ravishankara and P. J. Crutzen, *Journal of Geophysical Research: Atmo-*

- spheres, 1997, 102, 12819-12829.
- 16 S. J. Riley and K. R. Wilson, *Faraday Discussions of the Chemical Society*, 1972, **53**, 132–146.
- 17 D. L. Phillips, B. A. Lawrence and J. J. Valentini, *The Journal of Physical Chemistry*, 1991, **95**, 9085–9091.
- 18 Y. S. Kim, W. K. Kang, D.-C. Kim and K.-H. Jung, *The Journal of Physical Chemistry A*, 1997, **101**, 7576–7581.
- 19 M. E. Corrales, V. Loriot, G. Balerdi, J. González-Vázquez, R. de Nalda, L. Bañares and A. H. Zewail, *Physical Chemistry Chemical Physics*, 2014, 16, 8812–8818.
- 20 K. F. Chang, M. Reduzzi, H. Wang, S. M. Poullain, Y. Kobayashi, L. Barreau, D. Prendergast, D. M. Neumark and S. R. Leone, *Nature Communications*, 2020, 11, 4042.
- 21 K. F. Chang, H. Wang, S. M. Poullain, J. González-Vázquez, L. Bañares, D. Prendergast, D. M. Neumark and S. R. Leone, The Journal of Chemical Physics, 2022, 156, 114304.
- 22 M. A. Todt, S. Datta, A. Rose, K. Leung and H. F. Davis, *Physical Chemistry Chemical Physics*, 2020, **22**, 27338–27347.
- 23 F. Godwin, C. Paterson and P. Gorry, *Molecular Physics*, 1987, **61**, 827–848.
- 24 Y. Liu, Q. Zheng, Y. Zhang, R. Zhang, Y. Wang and B. Zhang, ChemPhysChem, 2009, 10, 830–834.
- 25 F. Zhand, Y.-M. Wang, B. Zhang and W.-L. Feng, *Acta Physico-Chimica Sinica*, 2010, **26**, 1903–1908.
- 26 P. L. Ross and M. V. Johnston, *The Journal of Physical Chemistry*, 1995, **99**, 4078–4085.
- 27 B. Erk, R. Boll, S. Trippel, D. Anielski, L. Foucar, B. Rudek, S. W. Epp, R. Coffee, S. Carron, S. Schorb *et al.*, *Science*, 2014, 345, 288–291.
- 28 H. Ryufuku, K. Sasaki and T. Watanabe, *Physical Review A*, 1980, **21**, 745.
- 29 A. Niehaus, *Journal of Physics B: Atomic and Molecular Physics*, 1986, **19**, 2925.
- 30 R. Boll, B. Erk, R. Coffee, S. Trippel, T. Kierspel, C. Bomme, J. D. Bozek, M. Burkett, S. Carron, K. R. Ferguson *et al.*, *Structural Dynamics*, 2016, **3**, 043207.
- 31 K. Amini, E. Savelyev, F. Brauße, N. Berrah, C. Bomme, M. Brouard, M. Burt, L. Christensen, S. Düsterer, B. Erk *et al.*, *Structural Dynamics*, 2018, **5**, 014301.
- 32 F. Allum, N. Anders, M. Brouard, P. Bucksbaum, M. Burt, B. Downes-Ward, S. Grundmann, J. Harries, Y. Ishimura, H. Iwayama et al., Faraday Discussions, 2021, 228, 571–596.
- 33 F. Allum, V. Music, L. Inhester, R. Boll, B. Erk, P. Schmidt, T. M. Baumann, G. Brenner, M. Burt, P. V. Demekhin *et al.*, *Communications chemistry*, 2022, **5**, 42.
- 34 H. Köckert, J. W. Lee, F. Allum, K. Amini, S. Bari, C. Bomme, F. Brauße, M. Brouard, M. Burt, B. C. De Miranda *et al.*, *Journal of Physics B: Atomic, Molecular and Optical Physics*, 2022, 55, 014001.
- 35 T. Walmsley, J. Unwin, F. Allum, S. Bari, R. Boll, K. Borne, M. Brouard, P. Bucksbaum, N. Ekanayake, B. Erk et al., The Journal of Chemical Physics, 2023, 159, 144302.
- 36 J. Unwin, W. O. Razmus, F. Allum, J. R. Harries, Y. Kumagai, K. Nagaya, M. Britton, M. Brouard, P. Bucksbaum, M. Fushi-

- tani et al., ACS Physical Chemistry Au, 2024, 4, 620-631.
- 37 F. Allum, Y. Kumagai, K. Nagaya, J. Harries, H. Iwayama, M. Britton, P. H. Bucksbaum, M. Burt, M. Brouard, B. Downes-Ward *et al.*, *Physical Review A*, 2023, **108**, 043113.
- 38 H. Fukuzawa, K. Nagaya and K. Ueda, Nuclear Instruments and Methods in Physics Research Section A: Accelerators, Spectrometers, Detectors and Associated Equipment, 2018, 907, 116 131.
- 39 J. W. McManus, T. Walmsley, K. Nagaya, J. R. Harries, Y. Kumagai, H. Iwayama, M. N. Ashfold, M. Britton, P. H. Bucksbaum, B. Downes-Ward et al., Physical Chemistry Chemical Physics, 2022, 24, 22699–22709.
- 40 T. Walmsley, J. W. McManus, Y. Kumagai, K. Nagaya, J. Harries, H. Iwayama, M. N. Ashfold, M. Britton, P. H. Bucksbaum, B. Downes-Ward *et al.*, *The Journal of Physical Chemistry A*, 2024, 128, 4548–4560.
- 41 W. O. Razmus, F. Allum, J. Harries, Y. Kumagai, K. Nagaya, S. Bhattacharyya, M. Britton, M. Brouard, P. H. Bucksbaum, K. Cheung et al., Physical Chemistry Chemical Physics, 2024, 26, 12725–12737.
- 42 N. Saito and I. H. Suzuki, *International Journal of Mass Spectrometry and Ion Processes*, 1992, **115**, 157–172.
- 43 T. N. Olney, G. Cooper and C. Brion, *Chemical physics*, 1998, **232**, 211–237.
- 44 S. Owada, K. Togawa, T. Inagaki, T. Hara, T. Tanaka, Y. Joti, T. Koyama, K. Nakajima, H. Ohashi, Y. Senba, T. Togashi, K. Tono, M. Yamaga, H. Yumoto, M. Yabashi, H. Tanaka and T. Ishikawa, *Journal of Synchrotron Radiation*, 2018, 25, 282–288.

- 45 S. Owada, K. Nakajima, T. Togashi, T. Katayama, H. Yumoto, H. Ohashi and M. Yabashi, *Journal of Synchrotron Radiation*, 2019, 26, 887–890.
- 46 A. T. J. B. Eppink and D. H. Parker, Review of Scientific Instruments, 1997, 68, 3477–3484.
- 47 A. Kramida, Yu. Ralchenko, J. Reader and and NIST ASD Team, NIST Atomic Spectra Database (ver. 5.12), [Online]. Available: https://physics.nist.gov/asd [2025, May 19]. National Institute of Standards and Technology, Gaithersburg, MD., 2024.
- 48 F. Ziaee, K. Borne, R. Forbes, Y. Malakar, B. Kaderiya, T. Severt, I. Ben-Itzhak, A. Rudenko, D. Rolles *et al.*, *Physical Chemistry Chemical Physics*, 2023, **25**, 9999–10010.
- 49 Y. Liu, T. Rozgonyi, P. Marquetand and T. Weinacht, *The Journal of Chemical Physics*, 2020, **153**, 184304.
- 50 J. Dyke, A. Ellis, N. Jonathan and A. Morris, *Journal of the Chemical Society, Faraday Transactions 2: Molecular and Chemical Physics*, 1985, **81**, 1573–1586.
- 51 W. Koch, B. Liu and P. v. R. Schleyer, *Journal of the American Chemical Society*, 1989, 111, 3479–3480.
- 52 S. Chelkowski, P. Corkum and A. Bandrauk, *Physical review letters*, 1999, **82**, 3416.
- 53 J. Unwin, F. Allum, M. Britton, I. Gabalski, H. Bromberger, M. Brouard, P. H. Bucksbaum, T. Driver, N. Ekanayake, D. Garg et al., Communications Physics, 2023, 6, 309.
- 54 F. Ziaee, Imaging nuclear motion during the photofragmentation of halomethane molecules triggered by ultraviolet light, Kansas State University, 2022.

12 |